9

Approximate–State Riemann Solvers

9.1 Introduction

The method of Godunov [216] and its high–order extensions require the solution of the Riemann problem. In a practical computation this is solved billions of times, making the Riemann problem solution process the single most demanding task in the numerical method. In Chap. 4 we provided exact Riemann solvers for the Euler equations for ideal and covolume gases. An iterative procedure is always involved and the associated computational effort may not always be justified. This effort may increase dramatically by equations of state of complicated algebraic form or by the complexity of the particular system of equations being solved, or both. Approximate, non–iterative solutions have the potential to provide the necessary items of information for numerical purposes. There are essentially two ways of extracting approximate information from the solution of the Riemann problem to be used in Godunov–type methods: one approach is to find an *approximation to the numerical flux* employed in the numerical method, directly, see Chaps. 10, 11 and 12; the other approach is to find an *approximation to a state* and then evaluate the physical flux function at this state. It is the latter route the one we follow in this chapter.

We present, approximate, Riemann solvers that do not need an iteration process. We provide an approximate *solution for the state* required to evaluate the Godunov flux. The approximations can be used directly in the first–oder Godunov method and its high–order extensions. Some of the approximations presented are exceedingly simple but not accurate enough to produce *robust numerical methods*. This difficulty is resolved by designing *hybrid schemes* that combine various approximate solvers in and adaptive fashion. There are other uses of the explicit approximate solutions presented here. For instance, the simplest solutions can be used in the *characteristic limiting* of high–order Godunov type methods based on the MUSCL approach; see Sect. 13.4 of Chap. 13. They also provide valuable information of use in other well known approximate Riemann solvers. For instance, Roe's approximate Riemann solver, [407]

E.F. Toro, *Riemann Solvers and Numerical Methods for Fluid Dynamics*,
DOI 10.1007/b7976-1_9,

to be studied in Chap. 11, requires an entropy fix; the results of this chapter may be used to provide the state values in the Harten–Hyman entropy fix [243]. The approximate Riemann solver of Osher [372], to be studied in Chap. 12, requires intersection points for the integration paths; the approximations of this chapter can be used directly. The HLL approach of Harten, Lax and van Leer [244] for deriving approximate solutions to the Riemann problem, to be studied in Chap. 10, requires estimates for the smallest and largest signal velocities in the Riemann problem; again, the pressure–velocity approximation of this chapter can directly lead to estimates for wave speeds. The approximate solutions presented in this chapter may also be of use in other computational approaches, such as in *front tracking schemes* [468], [403]. The techniques discussed here can easily be extended to other systems, such as the shallow water equations, the steady supersonic Euler equations, the artificial compressibility equations (see Sect. 1.6.3 of Chap. 1) and the Euler equations with general equation of state.

Useful background for studying this chapter is found in Chaps. 2, 3, 4, and 6. The rest of this chapter is organised as follows: in Sect. 9.2 we recall the Godunov flux and the Riemann problem solution, in Sect. 9.3 we present very simple Riemann solvers based on primitive variable formulations of the Euler equations. In Sect. 9.4 we study approximations based on the exact function for pressure, namely the two–rarefaction approximation and the two–shock approximation. Hybrid schemes are dealt with in Sect. 9.5 and numerical results are presented in Sect. 9.6.

9.2 The Riemann Problem and the Godunov Flux

We want to solve numerically the general Initial Boundary Value Problem (IBVP)

$$\left.\begin{array}{ll} \text{PDEs} : \mathbf{U}_t + \mathbf{F}(\mathbf{U})_x = \mathbf{0} \ , \\ \text{ICs} \quad : \mathbf{U}(x,0) = \mathbf{U}^{(0)}(x) \ , \\ \text{BCs} \quad : \mathbf{U}(0,t) = \mathbf{U}_{\text{l}}(t) \ , \ \mathbf{U}(L,t) = \mathbf{U}_{\text{r}}(t) \ , \end{array}\right\} \tag{9.1}$$

utilising the explicit conservative formula

$$\mathbf{U}_i^{n+1} = \mathbf{U}_i^n + \frac{\Delta t}{\Delta x}[\mathbf{F}_{i-\frac{1}{2}} - \mathbf{F}_{i+\frac{1}{2}}] \ , \tag{9.2}$$

along with the Godunov intercell numerical flux

$$\mathbf{F}_{i+\frac{1}{2}} = \mathbf{F}(\mathbf{U}_{i+\frac{1}{2}}(0)) \ . \tag{9.3}$$

We assume that the solution of IBVP (9.1) exists. Here $\mathbf{U}_{i+\frac{1}{2}}(0)$ is the similarity solution $\mathbf{U}_{i+\frac{1}{2}}(x/t)$ of the Riemann problem

$$\left.\begin{array}{l} \mathbf{U}_t + \mathbf{F}(\mathbf{U})_x = \mathbf{0} \ , \\ \mathbf{U}(x,0) = \left\{ \begin{array}{l} \mathbf{U}_{\text{L}} \text{ if } x < 0 \ , \\ \mathbf{U}_{\text{R}} \text{ if } x > 0 \ , \end{array} \right. \end{array}\right\} \tag{9.4}$$

evaluated at $x/t = 0$. Fig. 9.1 shows the structure of the exact solution of the Riemann problem for the x–split three–dimensional Euler equations, for which the vectors of conserved variables and fluxes are

$$\mathbf{U} = \begin{bmatrix} \rho \\ \rho u \\ \rho v \\ \rho w \\ E \end{bmatrix} \quad , \quad \mathbf{F} = \begin{bmatrix} \rho u \\ \rho u^2 + p \\ \rho uv \\ \rho uw \\ u(E+p) \end{bmatrix} \quad . \tag{9.5}$$

The value $x/t = 0$ for the Godunov flux corresponds to the t–axis. See Chap. 6 for details. The piece–wise constant initial data, in terms of primitive variables, is

$$\mathbf{W}_L = \begin{bmatrix} \rho_L \\ u_L \\ v_L \\ w_L \\ p_L \end{bmatrix} \quad , \quad \mathbf{W}_R = \begin{bmatrix} \rho_R \\ u_R \\ v_R \\ w_R \\ p_R \end{bmatrix} \quad . \tag{9.6}$$

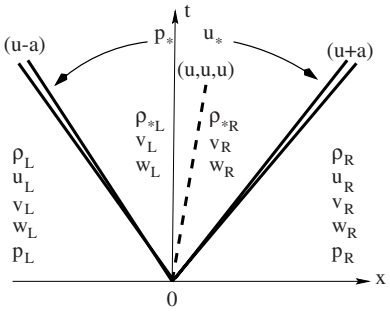

Fig. 9.1. Structure of the solution of the Riemann problem for the x–split, three dimensional Euler equations. Data and solution are given in terms of primitive variables

The purpose of this chapter is to find *approximate* solutions to the Riemann problem in order to evaluate the Godunov flux. As seen in Chap. 6, the evaluation of the flux requires the identification of the appropriate wave pattern in the Riemann problem solution; as depicted in Fig. 9.2, there are ten possibilities to be considered.

In our solution procedure we split the task of solving the complete Riemann problem into three subproblems, namely

(I) The star values

$$p_* \ , u_* \ , \rho_{*L} \ , \rho_{*R} \tag{9.7}$$

in the *Star Region* between the non–linear waves, see Fig. 9.1.

(II) The solution for the tangential velocity components v and w throughout the wave structure, and
(III) The solution for ρ, u and p inside sonic rarefactions.

Cases (II) and (III) are dealt with in the rest of this section, while case (I) is the subject of the rest of the chapter.

9.2.1 Tangential Velocity Components

Recall that in the exact solution, the values of the tangential velocity components v and w do not change across the non–linear waves but do change, discontinuously, across the *middle* wave. Thus, given an approximate solution u_* for the normal velocity component in the *Star Region*, the solution for the tangential velocity components v and w is

$$v(x,t)\ , w(x,t) = \begin{cases} v_L\ , w_L \text{ if } \frac{x}{t} \leq u_*\ , \\ \\ v_R\ , w_R \text{ if } \frac{x}{t} > u_*\ . \end{cases} \tag{9.8}$$

In this way, the solution for the tangential velocity components is, in a sense, *exact*; the only approximation being that for u_*. As a matter of fact, any *passive* scalar quantity $q(x,y,z,t)$ advected with the fluid will have this property. In the study of multi–component flow, this quantity could be a species concentration; in practical applications there can be many of such quantities. Hence, it is very important that the approximate solution of the Riemann problem preserves the correct behaviour, as in (9.8).

9.2.2 Sonic Rarefactions

Assuming the solution for the star values (9.7) is available, we then need to identify the correct values along the t–axis, in order to evaluate the Godunov flux. The cases (a1) to (a4) and (b1) to (b4) of Fig. 9.2 can be dealt with once solutions for (9.7) and (9.8) are available. The *sonic flow* cases (a5) and (b5) must be treated separately. For these two cases we recommend the use of the exact solution, which, as seen in Sect. 4.4 of Chap. 4 for ideal gases, is non–iterative.

The solution along the t–axis inside a *left sonic rarefaction* is obtained by setting $x/t = 0$ in

$$\mathbf{W}_{\text{Lfan}} = \begin{cases} \rho = \rho_{\text{L}} \left[\frac{2}{(\gamma+1)} + \frac{(\gamma-1)}{(\gamma+1)a_{\text{L}}} \left(u_{\text{L}} - \frac{x}{t} \right) \right]^{\frac{2}{\gamma-1}}\ , \\ \\ u = \frac{2}{(\gamma+1)} \left[a_{\text{L}} + \frac{(\gamma-1)}{2} u_{\text{L}} + \frac{x}{t} \right]\ , \\ \\ p = p_{\text{L}} \left[\frac{2}{(\gamma+1)} + \frac{(\gamma-1)}{(\gamma+1)a_{\text{L}}} \left(u_{\text{L}} - \frac{x}{t} \right) \right]^{\frac{2\gamma}{\gamma-1}}\ . \end{cases} \tag{9.9}$$

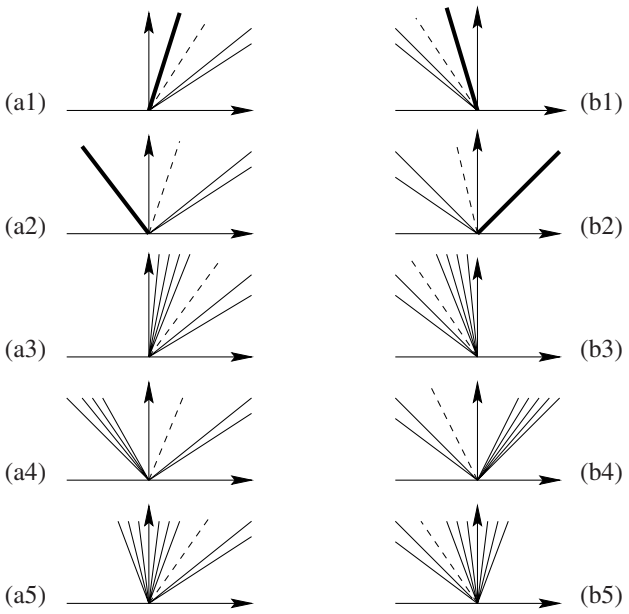

Fig. 9.2. Possible wave patterns in evaluating the Godunov flux for the Euler equations:(a) positive particle speed in the Star Region (b) negative particle speed in the Star Region

The solution along the t–axis inside a *right sonic rarefaction* is obtained by setting $x/t = 0$ in

$$\mathbf{W}_{\mathrm{Rfan}} = \begin{cases} \rho = \rho_{\mathrm{R}} \left[\frac{2}{(\gamma+1)} - \frac{(\gamma-1)}{(\gamma+1)a_{\mathrm{R}}} \left(u_{\mathrm{R}} - \frac{x}{t} \right) \right]^{\frac{2}{\gamma-1}} , \\ u = \frac{2}{(\gamma+1)} \left[-a_{\mathrm{R}} + \frac{(\gamma-1)}{2} u_{\mathrm{R}} + \frac{x}{t} \right] , \\ p = p_{\mathrm{R}} \left[\frac{2}{(\gamma+1)} - \frac{(\gamma-1)}{(\gamma+1)a_{\mathrm{R}}} \left(u_{\mathrm{R}} - \frac{x}{t} \right) \right]^{\frac{2\gamma}{\gamma-1}} . \end{cases} \tag{9.10}$$

The rest of this chapter is devoted to providing approximate solutions for the *star values* (9.7). We study four approaches as well as two adaptive schemes that combine various approximations.

9.3 Primitive Variable Riemann Solvers (PVRS)

A very simple linearised solution to the Riemann problem [502] for the x–split, three dimensional time dependent Euler equations (9.4)–(9.5) can be obtained in terms of the primitive variables ρ, u, v, w, p. The corresponding governing equations, see Sect. 3.2.3 of Chap. 3, are

$$\mathbf{W}_t + \mathbf{A}(\mathbf{W})\mathbf{W}_x = \mathbf{0}\ , \tag{9.11}$$

where the coefficient matrix $\mathbf{A}(\mathbf{W})$ is given by

$$\mathbf{A} = \begin{bmatrix} u & \rho & 0 & 0 & 0 \\ 0 & u & 0 & 0 & 1/\rho \\ 0 & 0 & u & 0 & 0 \\ 0 & 0 & 0 & u & 0 \\ 0 & \rho a^2 & 0 & 0 & u \end{bmatrix}\ . \tag{9.12}$$

The eigenvalues of $\mathbf{A}(\mathbf{W})$ are

$$\lambda_1 = u - a\ ,\ \lambda_2 = \lambda_3 = \lambda_4 = u\ ,\ \lambda_5 = u + a \tag{9.13}$$

and the matrix of corresponding right eigenvectors is

$$\mathbf{K} = \begin{bmatrix} \rho & 1 & \rho & \rho & \rho \\ -a & 0 & 0 & 0 & a \\ 0 & v & 1 & v & 0 \\ 0 & w & w & 1 & 0 \\ \rho a^2 & 0 & 0 & 0 & \rho a^2 \end{bmatrix}\ . \tag{9.14}$$

The difficulty in solving (9.11) is due to the fact that the coefficient matrix $\mathbf{A}(\mathbf{W})$ depends on the solution vector $\mathbf{W}$ itself. If $\mathbf{A}(\mathbf{W})$ were to be *constant*, then we could apply, directly, the various techniques studied in Sect. 2.3.3 of Chap. 2 for solving linear hyperbolic systems with constant coefficients.

Assume that the initial data $\mathbf{W}_L$, $\mathbf{W}_R$ and the solution $\mathbf{W}(x/t)$ are *close* to a constant state $\bar{\mathbf{W}}$. Then, by setting

$$\bar{\mathbf{A}} \equiv \mathbf{A}(\bar{\mathbf{W}}) \tag{9.15}$$

we approximate the Riemann problem for (9.11) by the Riemann problem for the linear hyperbolic systems with constant coefficients

$$\mathbf{W}_t + \bar{\mathbf{A}}\mathbf{W}_x = \mathbf{0}\ . \tag{9.16}$$

We now solve this *approximate problem*, with initial data (9.6), *exactly*. In Sect. 2.3.3 of Chap. 2 we studied various techniques that are directly applicable to this problem. One possibility is to apply Rankine–Hugoniot Conditions across each wave of speed $\bar{\lambda}_i$. Thus we treat (9.16) as the system in *conservative form*

$$\mathbf{W}_t + \mathbf{F}(\mathbf{W})_x = \mathbf{0}\ ,\quad \mathbf{F}(\mathbf{W}) \equiv \bar{\mathbf{A}}\mathbf{W}\ . \tag{9.17}$$

Then, across a wave of speed $\bar{\lambda}_i$ we have

$$\Delta\mathbf{F} \equiv \bar{\mathbf{A}}\Delta\mathbf{W} = \bar{\lambda}_i\Delta\mathbf{W}\ . \tag{9.18}$$

Direct application of (9.18) to the $\bar{\lambda}_1$ and $\bar{\lambda}_5$ waves gives four useful relations, namely

$$\left.\begin{array}{rl} (u_* - u_L)\bar{\rho} + \bar{a}(\rho_{*L} - \rho_L) &= 0\ , \\ (p_* - p_L)/\bar{\rho} + \bar{a}(u_* - u_L) &= 0\ , \\ (u_R - u_*)\bar{\rho} - \bar{a}(\rho_R - \rho_{*R}) &= 0\ , \\ (p_R - p_*)/\bar{\rho} - \bar{a}(u_R - u_*) &= 0\ . \end{array}\right\} \tag{9.19}$$

The complete solution for the unknowns (9.7) is then given by

$$\left.\begin{array}{rl} p_* &= \frac{1}{2}(p_L + p_R) + \frac{1}{2}(u_L - u_R)(\bar{\rho}\bar{a})\ , \\ u_* &= \frac{1}{2}(u_L + u_R) + \frac{1}{2}(p_L - p_R)/(\bar{\rho}\bar{a})\ , \\ \rho_{*L} &= \rho_L + (u_L - u_*)(\bar{\rho}/\bar{a})\ , \\ \rho_{*R} &= \rho_R + (u_* - u_R)(\bar{\rho}/\bar{a})\ . \end{array}\right\} \tag{9.20}$$

Notice that in this linearised solution we only need to specify constant values for $\bar{\rho}$ and $\bar{a}$. There is some freedom in making the choice. Selecting some average of the data values ρ_L, ρ_R, a_L, a_R appears sensible. The choice may be constrained to satisfy some desirable properties of the Riemann problem solution, such as exact recognition of particular flow features. Here we suggest to select the simple *arithmetic means*

$$\bar{\rho} = \frac{1}{2}(\rho_L + \rho_R)\ , \quad \bar{a} = \frac{1}{2}(a_L + a_R). \tag{9.21}$$

Note that if the data states $\mathbf{W}_L$ and $\mathbf{W}_R$ are connected by a *single isolated* contact discontinuity or shear wave, then the solution is actually *exact*, regardless of the particular choice for the averages $\bar{\rho}$ and $\bar{a}$. This is in fact a very important property; contacts and shear waves turn out to be some of the most challenging flow features to resolve correctly by any numerical method.

Another way of obtaining approximate solutions for the star values is to use the *characteristic equations*, see Sect. 3.1.2 of Chap. 3,

$$\mathrm{d}p - \rho a\,\mathrm{d}u = 0 \text{ along } \mathrm{d}x/\mathrm{d}t = u - a\ , \tag{9.22}$$

$$\mathrm{d}p - a^2\,\mathrm{d}\rho = 0 \text{ along } \mathrm{d}x/\mathrm{d}t = u\ , \tag{9.23}$$

$$\mathrm{d}p + \rho a\,\mathrm{d}u = 0 \text{ along } \mathrm{d}x/\mathrm{d}t = u + a\ . \tag{9.24}$$

These differential relations hold true *along characteristic* directions. First we set

$$C = \rho a. \tag{9.25}$$

Then, in order to find the star values we *connect* the state $\mathbf{W}_{*L}$ to the data state $\mathbf{W}_L$, see Fig. 9.1, by integrating (9.24) along the characteristic of speed $u + a$, where C is evaluated at the foot of the characteristic. See Fig. 9.3 The results is

$$p_* + C_L u_* = p_L + C_L u_L\ . \tag{9.26}$$

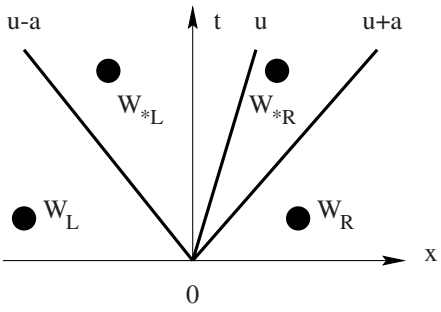

Fig. 9.3. Solution for star values using characteristic equations

Similarly, we connect $\mathbf{W}_{*R}$ to the data state $\mathbf{W}_R$ by integrating (9.22) along the characteristic of speed $u - a$, with C is evaluated at the foot of the characteristic. We obtain

$$p_* - C_R u_* = p_R - C_R u_R \; . \tag{9.27}$$

The values ρ_{*L} and ρ_{*R} are obtained by connecting $\mathbf{W}_{*L}$ to $\mathbf{W}_L$ and $\mathbf{W}_{*R}$ to $\mathbf{W}_R$ via (9.23). The complete solution is

$$\left.\begin{aligned} p_* &= \tfrac{1}{C_L+C_R}[C_R p_L + C_L p_R + C_L C_R (u_L - u_R)] \; , \\ u_* &= \tfrac{1}{C_L+C_R}[C_L u_L + C_R u_R + (p_L - p_R)] \; , \\ \rho_{*L} &= \rho_L + (p_* - p_L)/a_L^2 \; , \\ \rho_{*R} &= \rho_R + (p_* - p_R)/a_R^2 \; . \end{aligned}\right\} \tag{9.28}$$

In this approximation we do not need to make a choice for the averages $\bar{\rho}$ and $\bar{a}$; their values are replaced by data values at the foot of the corresponding characteristics. If $C_L = C_R = \bar{\rho}\bar{a}$, then the two approximations (9.20) and (9.28) are identical.

The two linearised approximations (9.20) and (9.28) for the star values are exceedingly simple and may be useful in a variety of ways. The approaches might prove very useful in solving the Riemann problem for complicated sets of equations.

We have now given the complete approximate solution to the sub–problems (9.7)–(9.10). In order to evaluate the Godunov flux (9.3) we need to *sample* the solution to find the value $\mathbf{W}_{i+\frac{1}{2}}(0)$ along the t–axis. This sampling procedure is virtually identical, although simpler, to the sampling procedure for the exact Riemann problem solution presented in Chap. 4. The reader is made aware that the numerical schemes associated with the simple linearised solutions just derived may not be robust enough to be used with absolute confidence under *all flow conditions*. In Sect. 9.5 we study hybrid Riemann solvers, which combine simple and sophisticated solvers to provide schemes that have effectively

the computational cost of the simplest Riemann solvers and the robustness of the sophisticated Riemann solvers.

9.4 Approximations Based on the Exact Solver

In Chap. 4 we presented an exact Riemann solver based on the pressure equation

$$f(p) \equiv f_L(p, \mathbf{W}_L) + f_R(p, \mathbf{W}_R) + \Delta u = 0 \ , \quad \Delta u = u_R - u_L \ , \tag{9.29}$$

with

$$f_K(p) = \begin{cases} (p - p_K) \left[\frac{A_K}{p + B_K} \right]^{\frac{1}{2}} \text{ if } p > p_K \text{ (shock)} \ , \\ \\ \frac{2a_K}{(\gamma - 1)} \left[\left(\frac{p}{p_K} \right)^z - 1 \right] \text{ if } p \leq p_K \text{ (rarefaction)} \ , \end{cases} \tag{9.30}$$

$$z = \frac{\gamma - 1}{2\gamma} \ , \quad A_K = \frac{2}{(\gamma + 1)\rho_K} \ , \quad B_K = \left(\frac{\gamma - 1}{\gamma + 1} \right) p_K \ , \quad K = L, R \ . \tag{9.31}$$

Various approximations based on $f(p) = 0$ can be obtained, including curve–fitting procedures [509]. Here we give approximations based on the rarefaction and shock branches (9.30) of $f(p)$.

9.4.1 A Two–Rarefaction Riemann Solver (TRRS)

Recall that the non–linear waves in the Riemann problem solution are either shock or rarefaction waves and finding their type is part of the solution procedure. If one assumes *a–priori that both non–linear waves are rarefactions* then (9.29), with the appropriate choice of f_L and f_R in (9.30), becomes

$$\frac{2a_L}{(\gamma - 1)} \left[\left(\frac{p}{p_L} \right)^z - 1 \right] + \frac{2a_R}{(\gamma - 1)} \left[\left(\frac{p}{p_R} \right)^z - 1 \right] + u_R - u_L = 0 \ .$$

Solving this equation for pressure p_* gives the approximation

$$p_* = \left[\frac{a_L + a_R - \frac{\gamma - 1}{2}(u_R - u_L)}{a_L / p_L^z + a_R / p_R^z} \right]^{\frac{1}{z}} \ . \tag{9.32}$$

Having found p_* one can obtain the particle velocity u_* from any of the rarefaction wave relations

$$u_* = u_L - \frac{2a_L}{(\gamma - 1)} \left[\left(\frac{p_*}{p_L} \right)^z - 1 \right] \tag{9.33}$$

or

$$u_* = u_R + \frac{2a_R}{(\gamma-1)}\left[\left(\frac{p_*}{p_R}\right)^z - 1\right] . \tag{9.34}$$

Alternatively, one can eliminate p_* from (9.33) and (9.34) to obtain a closed–form solution for the particle velocity

$$u_* = \frac{P_{LR}u_L/a_L + u_R/a_R + 2(P_{LR}-1)/(\gamma-1)}{P_{LR}/a_L + 1/a_R} , \quad P_{LR} = \left(\frac{p_L}{p_R}\right)^z . \tag{9.35}$$

Computing p_* from (9.32) requires the evaluation of 3 fractional powers. A more efficient approach is to calculate u_* from (9.35), which only requires one fractional power, and then evaluate p_* from (9.33) or (9.34), or from a mean value as

$$p_* = \frac{1}{2}\left\{p_L\left[1+\frac{(\gamma-1)}{2a_L}(u_L-u_*)\right]^{\frac{1}{z}} + p_R\left[1+\frac{(\gamma-1)}{2a_R}(u_*-u_R)\right]^{\frac{1}{z}}\right\} . \tag{9.36}$$

Being consistent with the assumption that the two nonlinear waves are rarefaction waves, the computation of the densities ρ_{*L} and ρ_{*R} on either side of the contact discontinuity is obtained from the isentropic law, see Sect. 3.1.2 of Chap. 3. The result is

$$\rho_{*L} = \rho_L\left(\frac{p_*}{p_L}\right)^{\frac{1}{\gamma}} , \quad \rho_{*R} = \rho_R\left(\frac{p_*}{p_R}\right)^{\frac{1}{\gamma}} . \tag{9.37}$$

An improved version of the two–rarefaction solution is obtained by using exact relations, for given p_* or u_*. For instance, suppose p_* is given by (9.32) say, then u_* can be found from

$$u_* = \frac{1}{2}(u_L+u_R) + \frac{1}{2}\left[f_R(p_*) - f_L(p_*)\right] , \tag{9.38}$$

where the functions f_L and f_R are evaluated according to the exact relations (9.30) by comparing p_* with p_L and p_R. The densities ρ_{*L} and ρ_{*R} can be found from the isentropic law if the K wave is a rarefaction ($p_* \le p_K$) or from the shock relation if the K wave is a shock wave ($p_* > p_K$).

The two–rarefaction approximation is generally quite robust; it is more accurate, although more expensive, than the simple PVRS solutions (9.20) or (9.28) of the previous section. The TRRS is in fact exact when both non–linear waves are actually rarefaction waves. This can be detected a–priori by the condition

$$f(p_{min}) \ge 0 \text{ with } p_{min} = \min(p_L, p_R) . \tag{9.39}$$

See Sect. 4.3 of Chap. 4 for details on the behaviour of the pressure function.

We have now given another approximate solution to the problem (9.7). The solution for (9.9)–(9.10) follows. The evaluation of the Godunov flux (9.3) requires sampling the solution to find the value $\mathbf{W}_{i+\frac{1}{2}}(0)$ along the t–axis, in the usual way. See Sect. 4.5 of Chap. 4.

9.4.2 A Two–Shock Riemann Solver (TSRS)

By assuming that *both non–linear waves are shock waves* in (9.29)–(9.30) one can derive the two–shock approximation

$$f(p) = (p - p_L)g_L(p) + (p - p_R)g_R(p) + u_R - u_L = 0 \,, \tag{9.40}$$

with

$$g_K(p) = \left[\frac{A_K}{p + B_K}\right]^{\frac{1}{2}} \tag{9.41}$$

and A_K, B_K given by (9.31). Unfortunately, this approximation does not lead to a closed–form solution. Further approximations must be constructed [168], [384], [509]. Obvious approximations to the two–shock approximation involve quadratic equations. These do not generally lead to robust schemes. One difficulty is the non–uniqueness of solutions and making the correct choice; the exact solution, as seen in Chap. 4, is unique. The other problem is the case of complex roots (non–existence) even for data for which the exact problem has a solution; in our experience these can occur very often and is therefore the most serious difficulty of the two–shock approach.

An alternative approach [509] is as follows. First we assume an estimate p_0 for the solution for pressure. Then we insert this estimate in the functions (9.41), which in turn are substituted into equation (9.40). We obtain

$$(p - p_L)g_L(p_0) + (p - p_R)g_R(p_0) + u_R - u_L = 0 \,.$$

The solution of this equation is immediate:

$$p_* = \frac{g_L(p_0)p_L + g_R(p_0)p_R - (u_R - u_L)}{g_L(p_0) + g_R(p_0)} \,. \tag{9.42}$$

Being consistent with the two–shock assumption we derive a solution for the velocity u_* as

$$u_* = \frac{1}{2}(u_L + u_R) + \frac{1}{2}\left[(p_* - p_R)g_R(p_0) - (p_* - p_L)g_L(p_0)\right] \,. \tag{9.43}$$

Solution values for $\rho_{*L} and \rho_{*R}$ obtained from shock relations, see Sect. 3.1.3 of Chap. 3, namely

$$\rho_{*L} = \rho_L \left[\frac{\frac{p_*}{p_L} + \frac{(\gamma-1)}{(\gamma+1)}}{\frac{(\gamma-1)}{(\gamma+1)}\frac{p_*}{p_L} + 1}\right] \,, \quad \rho_{*R} = \rho_R \left[\frac{\frac{p_*}{p_R} + \frac{(\gamma-1)}{(\gamma+1)}}{\frac{(\gamma-1)}{(\gamma+1)}\frac{p_*}{p_R} + 1}\right] \,. \tag{9.44}$$

As to the choice for the pressure estimate p_0 we propose

$$p_0 = max(0, p_{pvrs}) \,, \tag{9.45}$$

where p_{pvrs} is the solution (9.20) for pressure given by the PVRS solver of Sect. 9.3.

We have just presented another approximate solution to the problem (9.7). As before, the solution for (9.8)–(9.10) follows. The evaluation of the Godunov flux (9.3) requires sampling the solution to find the value $\mathbf{W}_{i+\frac{1}{2}}(0)$ along the t– axis, in the usual way. See Sect. 4.5 of Chap. 4.

The approximation (9.42)–(9.44) to the star values (9.7) is more efficient than the TRRS and only slightly more expensive than the PVRS approximations. Also TSRS is more accurate than TRRS and PVRS for a wider range of flow conditions, except for *near vacuum conditions*, where TRRS is very accurate or indeed exact. As for the case of the TRRS approximation, we can improve the TSRS by using the true wave relations whenever possible. For instance, for given p_* as computed from (9.42), one can obtain u_*, ρ_{*L} and ρ_{*R} from exact wave relations. This is bound to improve the accuracy of the derived quantities.

9.5 Adaptive Riemann Solvers

In a typical flow field the overwhelming majority of local Riemann problems are a representation for smooth flow. Large gradients occur only near shock waves, contact surfaces, shear waves or some other sharp flow features. Large gradients generate Riemann problems with *widely different data states* $\mathbf{W}_L, \mathbf{W}_R$. Generally, it is in this kind of situations where approximate Riemann solvers can be fatally inaccurate, leading to failure of the numerical method being used. The rationale behind the use of hybrid schemes is *the use of simple Riemann solvers in regions of smooth flow and near isolated contacts and shear waves, and more sophisticated Riemann solvers elsewhere, in an adaptive fashion.*

Successful implementations of adaptive schemes involving the PVRS and the exact Riemann solvers were presented in [502] for the two–dimensional, time dependent Euler equations. Toro and Chou [533] extended the idea to the case of the steady supersonic Euler equations. Quirk [400] implemented this Riemann–solver adaptation approach in a MUSCL–type scheme, used in conjunction with adaptive mesh refinement techniques.

Here we present two hybrid schemes to compute the star values (9.7). Problems (9.8)–(9.10) are solved as before and the sampling is handled as described in Sect. 4.5 of Chap. 4.

9.5.1 An Adaptive Iterative Riemann Solver (AIRS)

This adaptive scheme makes use of two Riemann solvers: any of the primitive–variable Riemann solvers PVRS of Sect. 9.3 and the exact Riemann solver of Chap. 4. The PVRS scheme is used if the following two conditions are met:

$$Q = p_{\max}/p_{\min} < Q_{\text{user}} \tag{9.46}$$

and

$$p_{\min} < p_* < p_{\max} \ , \tag{9.47}$$

where

$$p_{\min} \equiv \min(p_L, p_R) \ , \quad p_{\max} \equiv \max(p_L, p_R) \ , \quad p_* \equiv p_{pvrs} \ . \tag{9.48}$$

Otherwise, the exact Riemann solver is used.

Some remarks on the switching conditions (9.46)–(9.47) are in order. Condition (9.46) ensures that the pressure data values p_L, p_R are not widely different. Condition (9.47) imposes an extra restriction on the use of PVRS. The pressure restriction (9.46) is not sufficient; in fact for $Q \approx 1, (p_L \approx p_R)$ and $\Delta u = u_R - u_L$ negative and large in absolute value, strong shock waves are present in the solution of the Riemann problem, that is $p_* > p_{\max}$. For Δu large and positive $p_* < p_{\min}$ and strong rarefactions are present in the exact solution of the Riemann problem. Condition (9.47) is effectively a condition on Δu and excludes the two–rarefaction and the two–shock cases; both of these cases occur naturally at reflected boundaries, where it would be unwise to employ unreliable approximations. Also, these two cases are inconsistent with condition (9.46) on pressure ratios.

A choice of the switching parameter Q_{user} is to be made. Extensive testing suggests that the value $Q_{\text{user}} = 2$ is perfectly adequate to give both very robust and efficient schemes. Even much larger values of Q_{user} can give accurate solutions, but the gains are not significant and thus the cautious choice of $Q_{\text{user}} = 2$ is recommended. For typical flow conditions and meshes, over 90% of all Riemann problems are handled by the cheap linearised Riemann solver. Effectively, the resulting schemes have the efficiency of the cheapest Riemann solvers and the robustness of the exact Riemann solver. A disadvantage of this hybrid PVRS–EXACT scheme is the iterative character of the robust component of the scheme, namely the exact Riemann solver. This may be inconvenient for some computer architectures. One possibility here is to fix the number of iterations in the exact Riemann solver. In our experience, *one iteration* leads to very accurate values for pressure and subsequent quantities derived. This is due in part to the provision of a sophisticated starting value for the iteration procedure.

9.5.2 An Adaptive Noniterative Riemann Solver (ANRS)

Here we propose to combine a PVRS scheme, as the cheap component, together with the non–iterative TRRS and TSRS solvers of Sects. 9.4.1 and 9.4.2 to provide the robust component of the adaptive scheme. The use of PVRS is again restricted by conditions (9.46)–(9.47) of the previous scheme. If any of conditions (9.46) or (9.47) are not met we use either TRRS or TSRS. The switching between TRRS and TSRS is motivated by the behaviour of the exact function for pressure, see Sect. 4.3.1 of Chap. 4, and is as follows. If

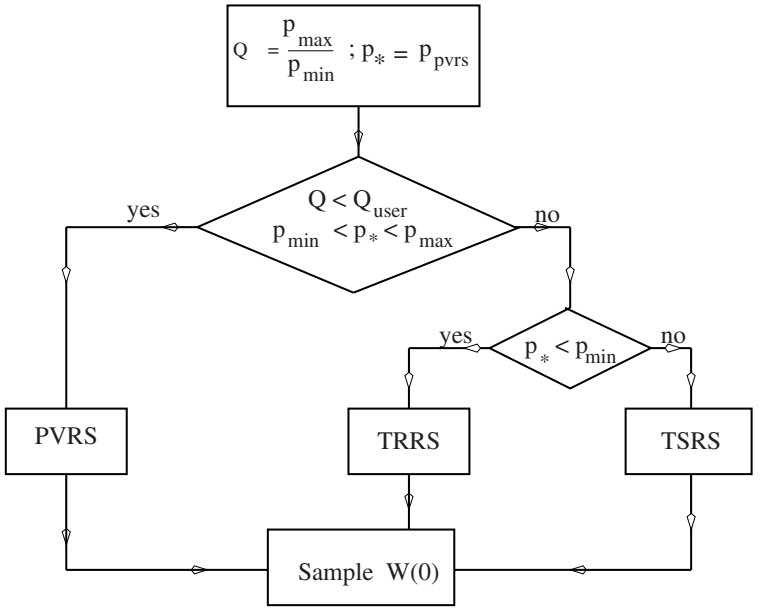

Fig. 9.4. Flow chart for Adaptive Noniterative Riemann Solver (ANRS) involving PVRS, TRRS and TSRS

$$p_{pvrs} \leq p_{\min} \ , \tag{9.49}$$

then we use TRRS, otherwise we use TSRS. The flow chart of Fig. 9.4 illustrates the implementation of this adaptive scheme. The problems of computing the tangential velocity components, handling sonic flow and the sampling procedure to find the Godunov flux are dealt with as described in the previous sections. This adaptive noniterative Riemann solver is recommended for practical applications.

9.6 Numerical Results

Here we assess the performance of Godunov's first–order upwind method used in conjunction with the approximate Riemann solvers presented in this chapter. We select five test problems for the one–dimensional, time dependent Euler equations for ideal gases with $\gamma = 1.4$; these have exact solutions, which are evaluated by running the code HE–E1RPEXACT of *NUMERICA* [519].

In all chosen tests, data consists of two constant states $\mathbf{W}_{\rm L} = [\rho_{\rm L}, u_{\rm L}, p_{\rm L}]^T$ and $\mathbf{W}_{\rm R} = [\rho_{\rm R}, u_{\rm R}, p_{\rm R}]^T$, separated by a discontinuity at a position $x = x_0$. The states $\mathbf{W}_{\rm L}$ and $\mathbf{W}_{\rm R}$ are given in Table 9.1. The ratio of specific heats is chosen to be $\gamma = 1.4$. For all test problems the spatial domain is the interval $[0, 1]$ which is discretised with $M = 100$ computing cells. The Courant number

coefficient is $C_{\text{cfl}} = 0.9$; boundary conditions are transmissive and $S^n_{\max}$ is found using the simplified formula (6.20) of Chapt. 6. But given that this formula is somewhat unreliable, see discussion of Sect. 6.3.2 of Chapter 6, in all computations presented here we take, for the the first 5 time steps, a Courant number coefficient C_{cfl} reduced by a factor of 0.2.

Test	ρ_{L}	u_{L}	p_{L}	ρ_{R}	u_{R}	p_{R}
1	1.0	0.75	1.0	0.125	0.0	0.1
2	1.0	-2.0	0.4	1.0	2.0	0.4
3	1.0	0.0	1000.0	1.0	0.0	0.01
4	5.99924	19.5975	460.894	5.99242	-6.19633	46.0950
5	1.0	-19.59745	1000.0	1.0	-19.59745	0.01

Table 9.1. Data for five test problems with exact solution. Test 5 is like Test 3 with negative uniform background speed

Test 1 is a *modified version* of the popular Sod's test [453]; the solution consists of a right shock wave, a right travelling contact wave and a left *sonic* rarefaction wave; this test is very useful in assessing the *entropy satisfaction* property of numerical methods. Test 2 has solution consisting of two symmetric rarefaction waves and a trivial contact wave of zero speed; the *Star Region* between the non–linear waves is close to vacuum, which makes this problem a suitable test for assessing the performance of numerical methods for low–density flows; this is the so called *123 problem* introduced in chapter Chap. 4. Test 3 is designed to assess the robustness and accuracy of numerical methods; its solution consists of a strong shock wave, a contact surface and a left rarefaction wave. Test 4 is also designed to test robustness of numerical methods; the solution consists of three strong discontinuities travelling to the right. See Sect. 4.3.3 of Chap. 4 for more details on the exact solution of these test problems. Test 5 is also designed to test the robustness of numerical methods but the main reason for devising this test is to assess the ability of the numerical methods to resolve *slowly– moving contact discontinuities*. The exact solution of Test 5 consists of a left rarefaction wave, a right–travelling shock wave and a *stationary* contact discontinuity. For each test we select a convenient position x_0 of the initial discontinuity and an output time. These are stated in the legend of each figure displaying computational results.

We present numerical results for two of the approximate Riemann solvers presented in this chapter, namely the Two–Shock Riemann solver (TSRS) and the Adaptive Noniterative Riemann Solver (ANRS). The numerical solutions are obtained by running the code HE–E1GODSTATE of *NUMERICA* [519]. The results from TSRS are shown in Figs. 9.5 to 9.9 and those of ANRS are shown in Figs. 9.10 to 9.14. All of these results are to be compared with those obtained from the Godunov scheme used in conjunction with the exact Riemann solver, see Figs. 6.8 to 6.12, Chapt. 6; to plotting accuracy, there is

no difference in the computed results. The two approximate Riemann solvers TSRS and ANRS are recommended for practical applications.

The Godunov–type methods based on the approximate–state Riemann solvers of this chapter are extended to second–order of accuracy using the techniques of Chaps. 13 and 14, for one–dimensional problems. Approaches for including source terms are given in Chapt. 15 and for solving multidimensional problems in Chap. 16.

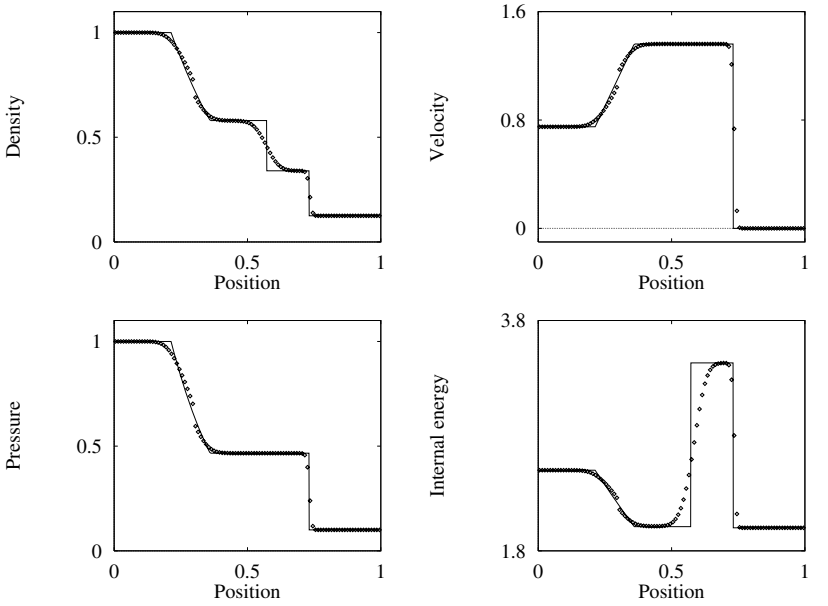

Fig. 9.5. Two–Shock Riemann Solver applied to Test 1, with $x_0 = 0.3$. Numerical (symbol) and exact (line) solutions are compared at time 0.2 units

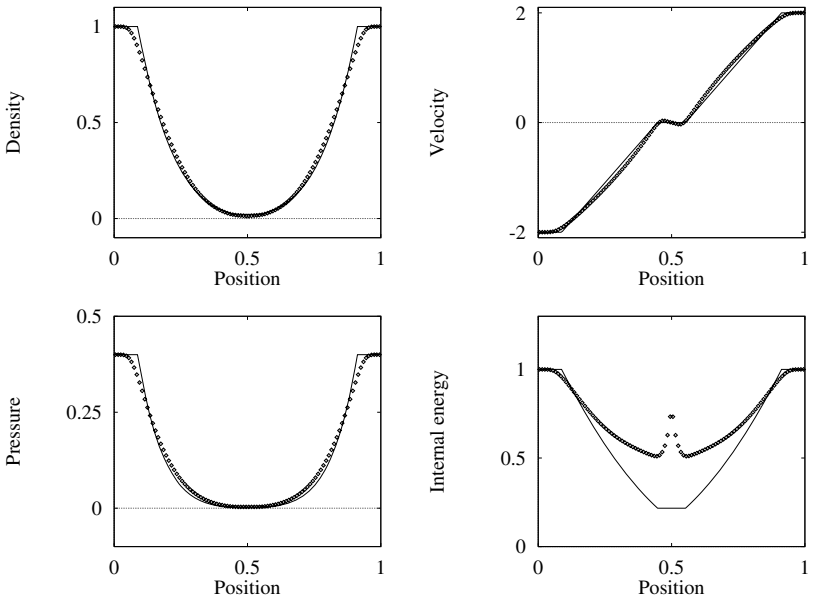

Fig. 9.6. Two–Shock Riemann Solver applied to Test 2, with $x_0 = 0.5$. Numerical (symbol) and exact (line) solutions are compared at time 0.15 units

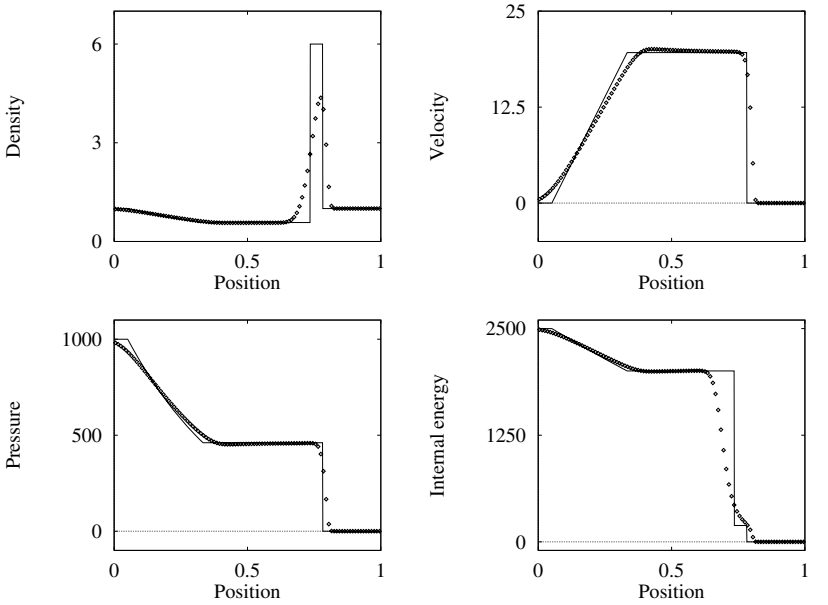

Fig. 9.7. Two–Shock Riemann Solver applied to Test 3, with $x_0 = 0.5$. Numerical (symbol) and exact (line) solutions are compared at time 0.012 units

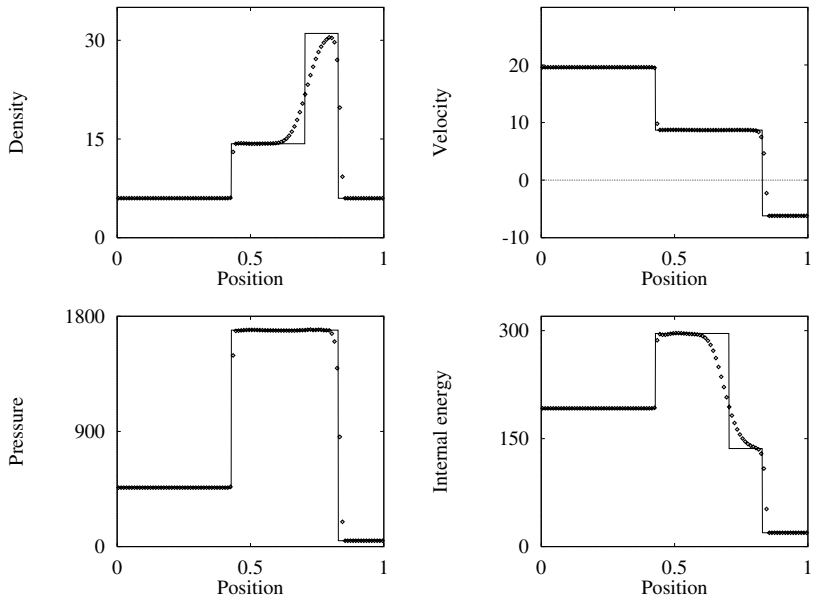

Fig. 9.8. Two–Shock Riemann Solver applied to Test 4, with $x_0 = 0.4$. Numerical (symbol) and exact (line) solutions are compared at time 0.035 units

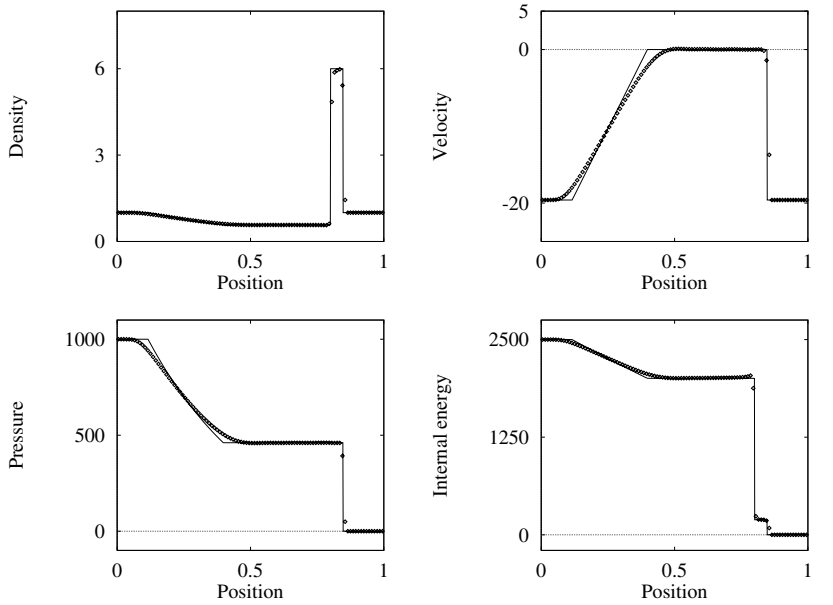

Fig. 9.9. Two–Shock Riemann Solver applied to Test 5, with $x_0 = 0.8$. Numerical (symbol) and exact (line) solutions are compared at time 0.012 units

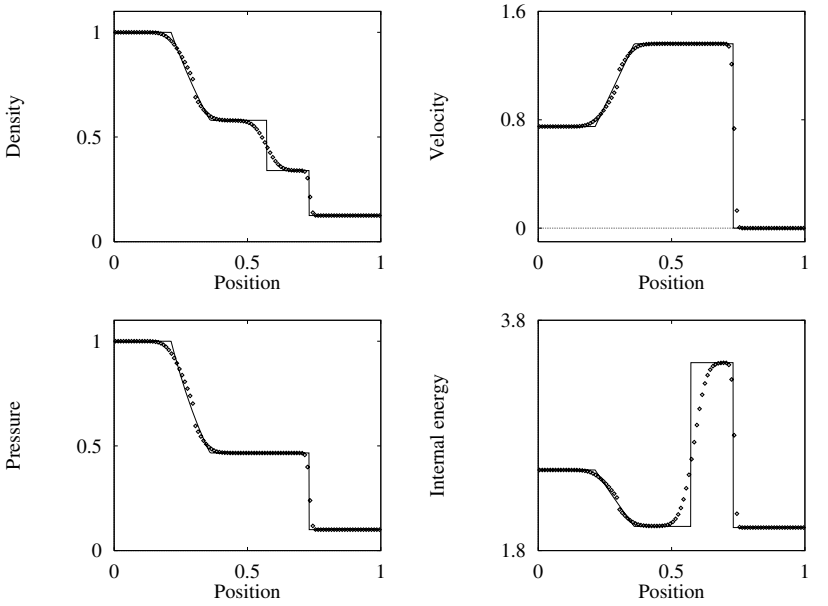

Fig. 9.10. Adaptive Noniterative Riemann Solver applied to Test 1, with $x_0 = 0.3$. Numerical (symbol) and exact (line) solutions are compared at time 0.2 units

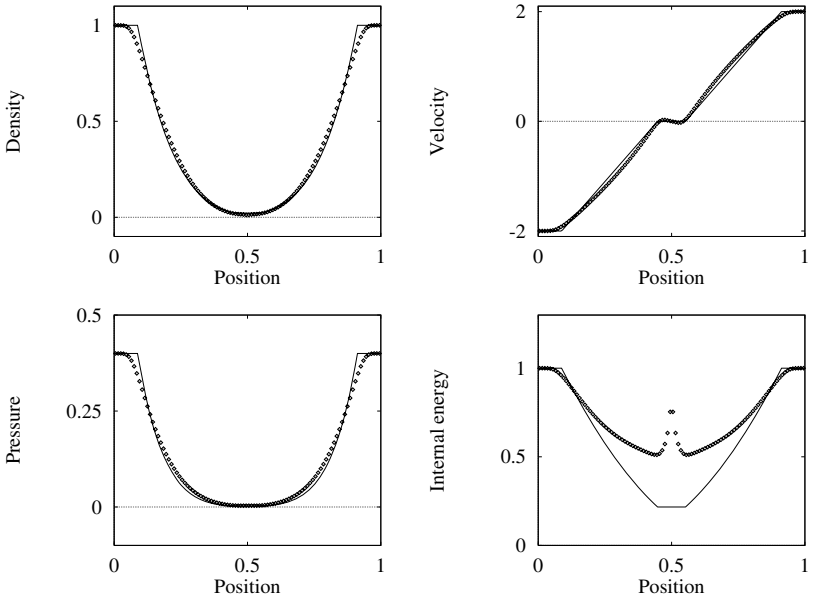

Fig. 9.11. Adaptive Noniterative Riemann Solver applied to Test 2, with $x_0 = 0.5$. Numerical (symbol) and exact (line) solutions are compared at time 0.15 units

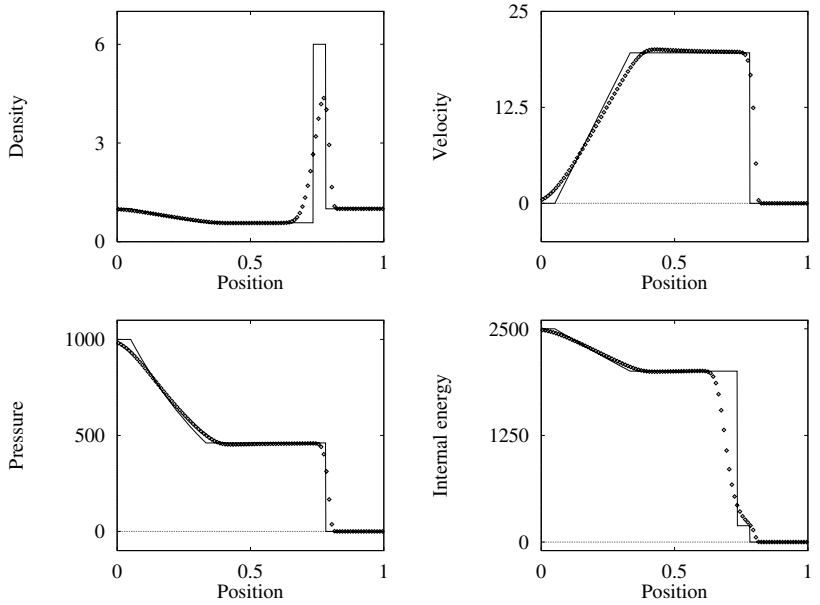

Fig. 9.12. Adaptive Noniterative Riemann Solver applied to Test 3, with $x_0 = 0.5$. Numerical (symbol) and exact (line) solutions are compared at time 0.012 units

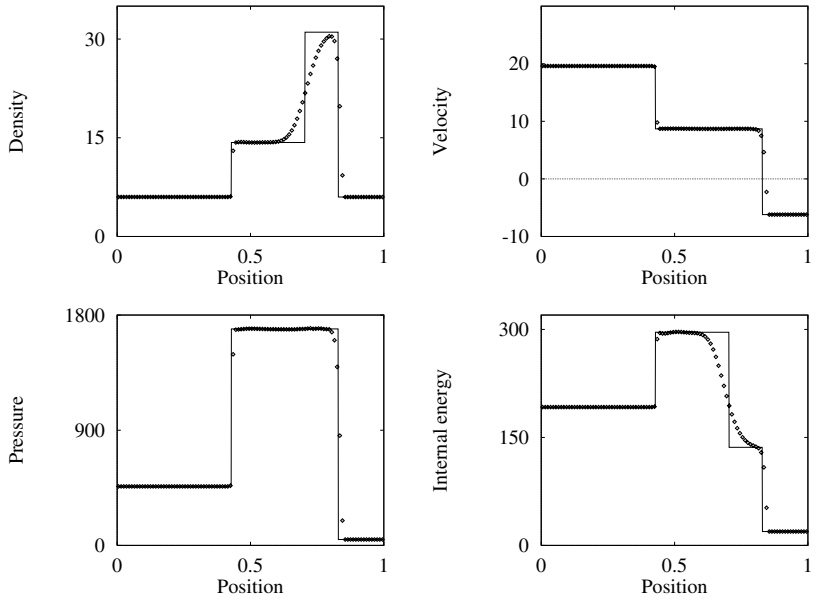

Fig. 9.13. Adaptive Noniterative Riemann Solver applied to Test 4, with $x_0 = 0.4$. Numerical (symbol) and exact (line) solutions are compared at time 0.035 units

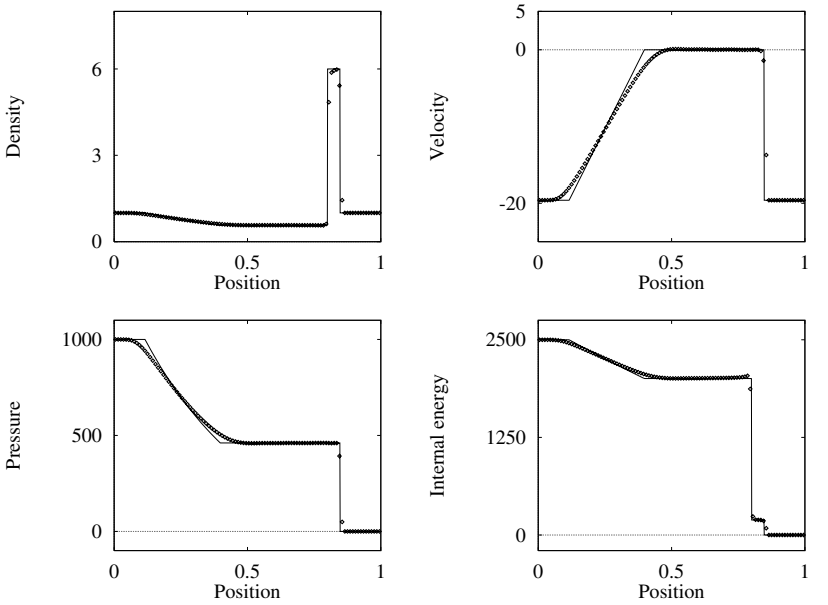

Fig. 9.14. Adaptive Noniterative Riemann Solver applied to Test 5, with $x_0 = 0.8$. Numerical (symbol) and exact (line) solutions are compared at time 0.012 units